A Dual-Polarized Reconfigurable Reflectarray with A Thin Liquid Crystal Layer and 2D Beam Scanning

Aghabeyki, Peyman; Cai, Yang; Deng, Guangsheng; Tan, Zheng-Hua; Zhang, Shuai

Published in:
I E E E Transactions on Antennas and Propagation

DOI (link to publication from Publisher):
10.1109/TAP.2023.3240853

Publication date:
2023

Document Version
Accepted author manuscript, peer reviewed version

A Dual-Polarized Reconfigurable Reflectarray with A Thin Liquid Crystal Layer and 2D Beam Scanning

Peyman Aghabeyki, *Student Member, IEEE,* Yang Cai, *Student Member, IEEE,* Guangsheng Deng, Zheng-Hua Tan, *Senior Member, IEEE* and Shuai Zhang, *Senior Member, IEEE*

***Abstract*—A novel approach for dual-polarized Liquid Crystal (LC) unit cell design is introduced, allowing significant thickness reduction of a LC layer without compromising its loss and phase shift. For each unit cell, LC is used for a tunable superstrate between a cross patch above and a square patch below. The square and cross patches are coupled through two slots for each polarization. By changing the voltage applied to the square and cross patches, the LC in-between varies the resonant frequency and phase of the unit cell to realize 2D beam steering. 10×10 dual-polarized reflectarray (RA) with 30 µm (0.0028 λ) and 4 µm (3.73×10^{-4} λ) thick LC layers are simulated in the 28 GHz band, where the aperture efficiencies (AE) are 25.3% and 22.5%, respectively. As a proof of concept, the dual-polarized RA with 30 µm thick LC is fabricated manually and measured at 28.5 GHz. A measurement technique is proposed to obtain the phase curves of the RA and reduce the effect of fabrication errors. With the imperfect manual fabrication, the RA still achieves the measured realized gain of 14.6 dBi corresponding to 12.5% AE. Besides, ±45° beam steering is demonstrated in the 2D plane for both polarizations.**

***Index Terms*— Beam-steering, dual polarization, liquid crystal, response time, reflectarray**

I. Introduction

RECONFIGURABLE reflectarrays (RA) have attracted great attention for their potential applications as satellite antennas, reconfigurable intelligent surfaces, and low-cost beam steerable arrays with high gain over the past years. In these applications, the capabilities of dual polarization and 2D beam steering are highly preferred. Different techniques have been developed to enable dynamic beam steering for them, such as PIN diodes [1], varactor diodes [2] and barium strontium titanate [3], and so on. Among them, liquid crystal (LC) is one of the most promising candidates due to its low cost for massive production with the existing Liquid Crystal Display (LCD) facilities. LC-based RAs use LC as the tuning substrate material that can change the reflective phase of the unit cell in the presence of applied voltage. Numerous studies have been carried out for LC-based unit cells with basic structures like square patches [4]-[6], multiple dipoles [7]-[9], and rectangular slots [10]. In addition, some other techniques were also exploited for LC-based unit cells [11][12]. In [11], a folded RA with a LC-based polarizing grid in the upper reflector was constructed, but the beam-steering was only limited to ±6 degrees at 78 GHz. LC was also implemented in aperture coupled delay lines to broaden the bandwidth of a RA with 2D scanning [12]. However, the unit cell size in [12] was large with single polarization and thick LC.

Despite the attractive LC features, the long response/ relaxation time of LC-based RAs limits their applications. In a simple LC capacitor, changing permittivity from $\varepsilon_{r\perp}$ (switch-off or relaxation) to $\varepsilon_{r||}$ (switch-on) is done by applying a variable voltage. Varying from $\varepsilon_{r||}$ to $\varepsilon_{r\perp}$ is achieved by applying extra voltage pads (fully electronically biasing) or using alignment layers (hybrid biasing) [13], which may take a much longer time than switching from "off" to "on" and is called response/ relaxation time. One major challenge in using LC in RA is that the long response time of a LC layer will limit the RA beam steering speed. Response time is proportional to the square of LC layer thickness [13]. Most of the previous studies utilized either thin LC at high frequencies of above 100 GHz or a thick LC layer below 100 GHz. In the conventional LC unit cell, LC is the main substrate and the patch is in the over-coupled state with a certain LC thickness, which is desirable for reflectarray applications [14]. As we decrease this desirable LC thickness, the patch first goes through a critically-coupled state which acts as an absorber, and then it goes through an under-coupled state which shows anomalous phase behavior and gives no phase shift. Therefore, the conventional arrangement of LC unit cells is very challenging to yield a low response time at relatively low frequencies. As a result, designing a LC-based unit cell is a compromise among loss, phase shift, and response time.

In recent years, several techniques have been used to reduce the thickness and response time of the LC in devices. Impurifying LC materials with various substances such as polymer networks [15] were proposed and showed significant improvements. However, these methods come with the cost of higher dielectric loss, lower anisotropy, and higher driving

The manuscript is received X. (Corresponding author: Shuai Zhang.)

Peyman Aghabeyki, Yang Cai, Zheng-Hua Tan, and Shuai Zhang are with the Department of Electronic Systems, Aalborg University, Aalborg, 9220, Denmark. (Email: sz@es.aau.dk)

Guangsheng Deng is with the Academy of Opto-Electric Technology, Hefei University of Technology, Hefei 230009, China.

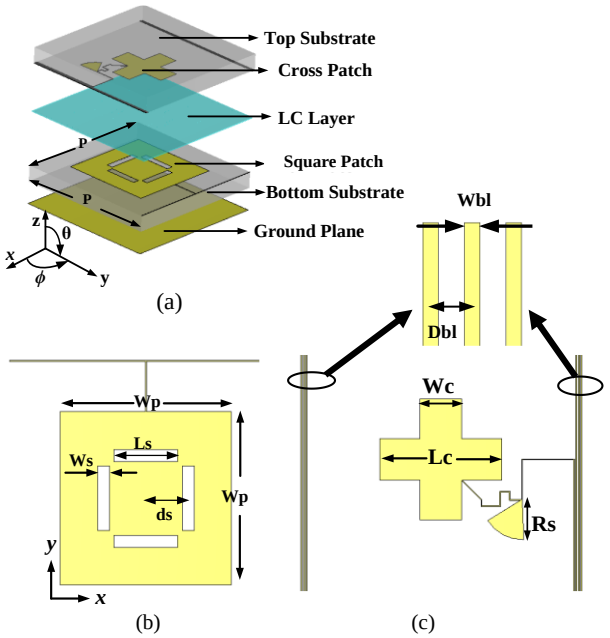

Fig. 1. Unit cell structure a) expanded view of layers b) square patch c) cross patch with bias lines. Wbl =15 µm, Dbl = 40 µm, Lc =1.94 mm Wc = 0.62 mm, Wp = 2.83 mm, ds = 0.7 mm, Rs = 0.6 mm, Ls = 1.05 mm, Ws = 0.22 mm P = 4.5 mm

voltage [13]. Rectangular slot elements with comb electrodes as the ground are used in [16] that realized a fully electronic biasing scheme in planar form. By overshooting the driving voltages, the need for low LC thickness can be avoided. However, due to inhomogeneous electric bias field in the LC substrate, tuning range of LC and phase shift are degraded. The work in [17] proposed a method of adding an extra square patch on top of a conventional LC-based patch unit cell. The added square patch makes a compromise between loss and phase shift. It keeps small LC thickness but reduces the phase shift and loss at the same time, which is not desirable. Although the LC thickness is reduced to 0.0075 λ (0.25 mm), the response time is still long, and the hybrid-biasing scheme may not be completely effective due to very thick LC layer at the relatively low frequencies. In addition, the issue of driving to under-coupled state by decreasing the LC layer also exists in this configuration. Similar to varactor delay lines in [13], a varactor-based unit cell is proposed in [18] that achieved 5.6×10^{-4} λ with 180° phase shift. However, the RA in [18] is only single-polarized and for 1-D beam steering with a low measured aperture efficiency of 5.8%.

It is a crucial task to seek innovative methods to further minimize LC thickness with satisfactory loss and phase shift as well as the capabilities of dual polarization and 2D scanning at millimeter-wave frequencies (especially below 60 GHz). In this work, we propose an innovative method for dual-polarized LC unit cell design in which the LC material is used on top of the conventional patch, as a substrate of a cross patch. Rectangular slots are also introduced in the square patch to couple the electric field between layers. The resonant frequency of the cross patch can be tuned by applying a bias voltage between patch metal layers. By using this technique, LC layer thickness can be decreased to 3.73×10^{-4} λ. As a proof of concept, a RA has also been simulated and fabricated with 30 µm (0.0028 λ) LC thickness and 2D beam steering capability. The performance of the RA prototype has been verified with measurements successfully. The rest of the paper is organized as follows: section II proposes a LC-based unit cell and elaborates on the working mechanism. Section III shows the simulated results of the designed reflectarray based on the proposed unit cells. Section IV discusses the fabrication of reflectarray and proposes a method for reflection phase testing. In Section V, the measured far-field radiation pattern is presented and discussed. Finally, a conclusion is drawn in Section VI.

II. Unit Cell Design

A. LC-based Unit Cell

Fig. 1 shows the proposed unit cell structure. From the bottom to the top, the first layer is a dielectric substrate with a ground plane and a square patch, the second layer is a thin liquid crystal layer, and the third layer is the dielectric substrate with a cross-shape patch on bottom face. In addition, two pairs of rectangular slots are etched on the main substrate. A thin bias line is connected to the cross patch through quarter wavelength line followed by a radial stub to choke the RF current. The point where the two arms of cross patch are joint has a very weak electric field, and thus adding the bias line has quite limited effects on the unit cell performance. Since we are using glass substrates, all the bias lines are printed on the bottom surface of the top glass substrate (see Fig. 1 (a)) to control each unit cell individually. To mimic the practical scenario of the unit cell, a couple of dummy bias lines are added near the main bias line (see Fig. 1 (c)). In addition, the square patch is connected to a narrow line, which connects all the unit cells to the ground of bias voltage. Before explaining the working mechanism of the UC, we need to illustrate how LC interacts with the RF field. The applied bias voltage between square patch and cross patch generates an electrostatic field that changes the permittivity of liquid crystal in between. If the electrostatic field is uniform in z-direction for a specific volume, we can assume that the permittivity tensor has the following form. Assuming the initial direction of LC directors in unbiased state is in the y direction, as the result of rubbing the polyimide alignment layer, the permittivity tensor is [13]:

$$\bar{\bar{\varepsilon}}_{V=0} = \begin{pmatrix} \varepsilon_{r\perp} & 0 & 0 \\ 0 & \varepsilon_{r\parallel} & 0 \\ 0 & 0 & \varepsilon_{r\perp} \end{pmatrix} \quad (1)$$

If a high-enough voltage is applied to the LC, the directors align in the z direction and, the permittivity tensor would be:

$$\bar{\bar{\varepsilon}}_{V\gg0} = \begin{pmatrix} \varepsilon_{r\perp} & 0 & 0 \\ 0 & \varepsilon_{r\perp} & 0 \\ 0 & 0 & \varepsilon_{r\parallel} \end{pmatrix} \quad (2)$$

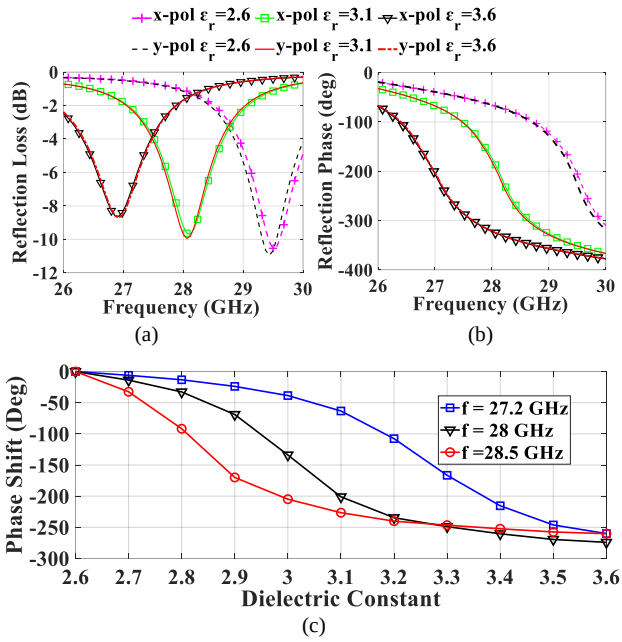

Fig. 2. x-pol and y-pol reflection a) magnitude and b) phase of proposed unit cell for different values of permittivity with 30 µm LC thickness. c) phase-permittivity curve for lower, center, and upper frequencies.

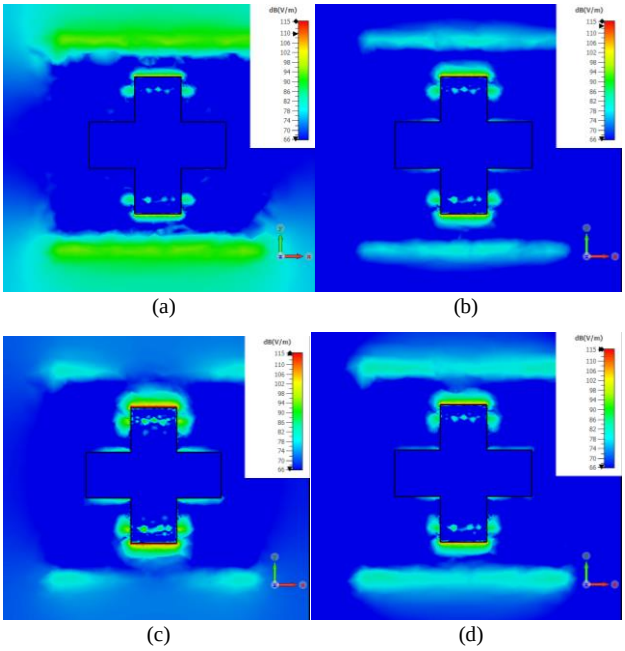

Fig. 3. Electric field distribution at a) 20 GHz b) 26 GHz c) 28 GHz d) 30 GHz between the cross and main patch of unit cell

Both substrates are 500-µm thickness fused silica with ε_r = 3.8 and tanδ = 0.002. Patches are designed with 1.5 µm copper layer. The measured dielectric range of the LC mixture that is used in this study is $\varepsilon_{r\perp}$ = 2.56 to $\varepsilon_{r\parallel}$ = 3.75 with tanδ ≈ 0.02 in the range of 100-140 GHz which is measured with metamaterial absorber [19]. Since the dielectric range was unknown at 28 GHz, we used the values of $\varepsilon_{r\perp}$ = 2.6 to $\varepsilon_{r\parallel}$ = 3.6 with tanδ = 0.02 in the simulation. The LC layer thickness is set to be h_{LC} = 30 µm which is equivalent to 0.0028λ at 28 GHz. To investigate the reflective behavior of the unit cell, the structure is simulated with Unit Cell boundary conditions in CST Microwave Studio. Note that to generate more accurate results, only the LC area below the cross patch is set with a variable permittivity since the electrostatic bias field is strong in this region, and the remaining LC area around the cross patch is set to constant unbiased state permittivity tensor as (1). Fig. 2 (a) and (b) shows the result of reflection amplitude and phase for y-polarized and x-polarized waves. As we increase the bias voltage, the permittivity of the LC layer changes from 2.6 to 3.6, and accordingly, resonant frequency decreases from 29.5 GHz to 26.9 GHz. Maximum loss is -11 dB, and 274˚of phase shift can be achieved which is enough for reflectarray applications. Since the geometry of the unit cell is symmetrical around x- and y-axis, two polarization responses are almost equal, and the small difference is mainly due to anisotropic nature of the LC material and bias lines. The LC anisotropic nature can be explained as follows: in the unbiased state, the whole unit cell shares the same anisotropic tensor, and the x and y permittivity are slightly different, so the difference for the x- and y-polarizations reach the maximum. However, in the fully biased state, x and y direction permittivity is the same, and thus x and y polarization are more similar. The largest discrepancy between two polarizations at 28 GHz is 8˚. Cross polarization is below -30 dB for all permittivity states, and it is not shown here for brevity.

To study the phase shift performance of the proposed unit cell across frequency, the upper and lower frequency limits are defined as the ones that have at least 260º phase shift. Based on this definition, f = 27.2 GHz and f = 28.5 GHz are the lower and upper frequencies, respectively. The curves of phase shift *vs* dielectric constant are demonstrated for lower, center, and upper frequencies in Fig. 2(c). It shows that the unit cell provides at least 260º phase shift over 1.3 GHz bandwidth.

To further investigate the working principle of the unit cell, electric field distribution on radiating edges of the unit cell is illustrated in Fig. 3 from 20 GHz to 30 GHz. The desired resonant frequency of the unit cell is around 28 GHz. The unit cell has two radiating edges. One of the associated resonant frequencies is from the square patch and the other is due to the cross patch. The resonant frequency of the square patch is around 20 GHz, and it is dominant at this frequency, as shown in Fig. 3(a). Fig. 3(b-d) shows the electric field at 26 GHz, 28 GHz, and 30 GHz, respectively. As the frequency increases to the resonant frequency of the cross patch at around 28 GHz, electric field at the cross-patch edges becomes stronger contributing more to the total reflection of the unit cell than that of the square patch. This is also the reason why we can change the resonant frequency by adjusting the LC permittivity. After 28 GHz, the electric field strength at the cross-patch edges increases again.

It is noticeable that for other patch configurations such as circular patch and slot similar magnitude and phase response

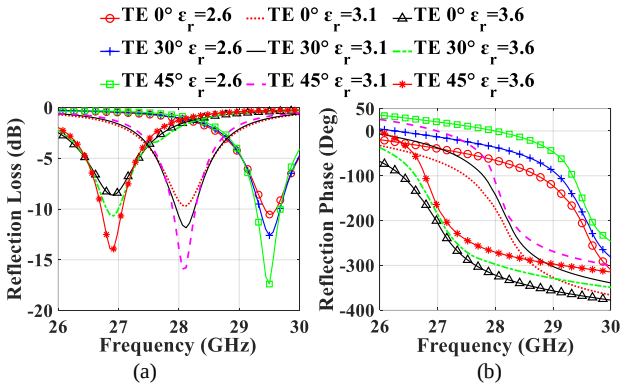

Fig. 4. Effect of changing incident angle on TE reflection a) magnitude and b) phase for unit cell with 30 µm LC thickness

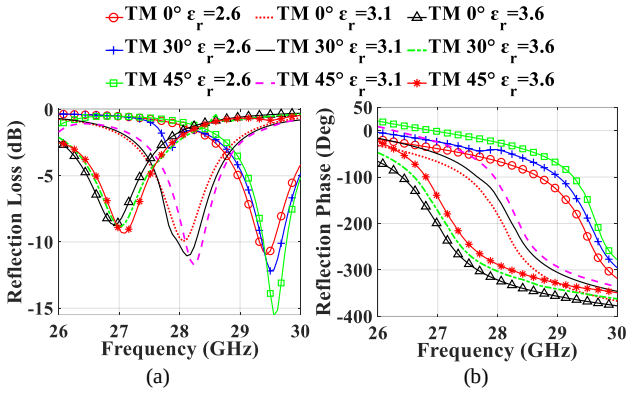

Fig. 5. Effect of changing incident angle on TM reflection a) magnitude and b) phase for unit cell with 30 µm LC thickness.

behaviors can be obtained if a proper physical dimension is adopted.

B. Oblique Incident

Often the unit cells are used in reflectarray with offset feeding scheme, so it would be informative to study the effect of Transverse Electric (TE) and Transverse Magnetic (TM) incident angle on the loss and phase shift of the proposed unit cell. Based on the coordinate system of Fig. 1, we set ϕ to be 90˚ and change θ of the incident angle from zero to 45˚. TE polarization is defined, as a wave that the electric field is orthogonal to the plane of incident, while TM is the wave the electric field is parallel to the plane of incident. Fig. 4 and 5 show the incident angle effect of TE and TM on reflection magnitude and phase for different permittivity values, respectively. For the TE case, as we increase the incident angle, the maximum reflection loss and phase increase from 11 dB to 17.5 dB and 274˚ to 300˚, respectively. On the other hand, for the TM case, as we increase the incident angle, the loss along with phase increases for low permittivity. However, as we increase the permittivity, the loss remains at the same level but with a slight change in frequency. In addition, due to the increased loss with lower permittivity, the TM wave phase shift is increased to 285˚ for the incident angle of 45˚. It is worth mentioning that the cross-polarization level remains below -25 dB for the entire range of incident angles.

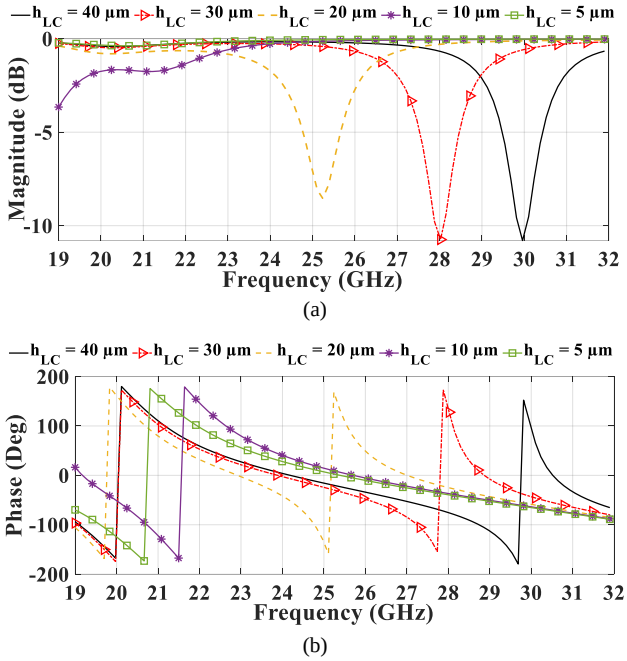

Fig. 6. Reflection a) magnitude and b) phase for different values of h_{LC} from 40 µm to 5-µm. rest of the unit cell dimensions are the same as Fig. 2.

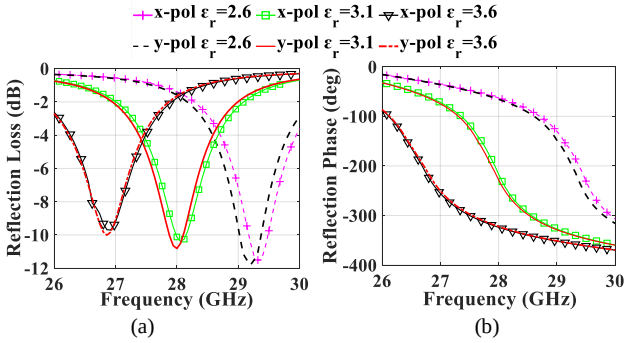

Fig. 7. Reflection a) magnitude and b) phase of the proposed unit cell for different values of permittivity with 4 µm LC thickness. Wbl =15 µm, Dbl = 40 µm, Lc =1.59 mm Wc = 0.55 mm, Wp = 2.95 mm, ds = 0.7 mm, Rs = 0.6 mm, Ls = 1.2 mm, Ws = 0.14 mm P = 4.5 mm

C. LC Thickness Reduction

The advantage of the proposed unit cell is that we can further reduce the thickness of the LC layer. Reflection magnitude and phase for h_{LC} = 40 µm, 30 µm, 20 µm, 10 µm, and 5 µm are displayed in Fig. 6. As the LC layer thickness reduces, the resonant frequency of the cross patch also decreases without a considerable effect on the square patch resonance. However, if we decrease the LC thickness further than h_{LC} = 10 µm, cross patch resonance nearly disappears due to a mismatch between the coupling slot and the cross patch. We can optimize the slot configurations and decrease the cross-patch dimensions to shift its resonant frequency to 28 GHz. Therefore, we fix the LC thickness of 4 µm and optimize other physical parameters to design a unit cell at 28 GHz. Fig. 7 shows the reflection magnitude and phase of the proposed unit cell for 4 µm LC thickness. As it is demonstrated in the figure, we can achieve 11.8 dB loss and

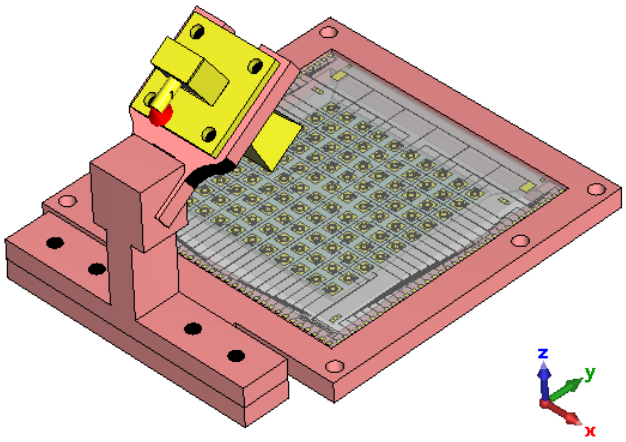

Fig. 8. Simulation setup of the proposed reflect array

270˚phase shift.

Therefore, we can achieve almost the same values for loss and phase shift with $h_{LC} = 3.73\times10^{-4}$ λ that is almost 8 times lower than the previous unit cell.

D. Response time

The loss, phase shift, and response time can be different depending on the types of LC. As an example, 30 µm thick LC of the HFUT-HB01 type would have approximately 200 ms switch-off response time [10]. However, if we use low-loss LC mixtures such as GT7 with 30 µm thickness, response time would be around 2 or 3 seconds [13] which can restrict the use of LC-based reflectarray in applications where agile beam-steering is needed. In LC-based reflectarray and phased array antennas, the beam-steering time would be shorter than the switch-off response time of the unit cells [13] because if we want to steer the beam between 2 given directions, not all the elements have to undergo the total cycle of permittivity range. It is worth mentioning that if we used GT7 as the tuning material of the proposed unit cell, reflection loss would be 4 dB lower than LC we used in this work with the same phase shift.

Moreover, as studied above, it is possible to use the proposed method to realize the unit cell with 4 µm thick LC at 28 GHz. If we use GT7 LC mixture (which has a low loss) with 4 µm thickness, the response time could be only around 30 ms [13], which would be suitable for practical applications. The curves of LC response time *vs* thickness for some of the well-known LC mixtures can be found in [13].

III. Reflectarray Design

To prove the capability of the proposed unit cells, 10 × 10 reflectarray on a glass substrate is designed and simulated for 30 µm LC thickness. The simulated setup is shown in Fig. 8 in which all the bias lines, soldering pads, horn fixture and marginal glass substrates are included in the model. In this study, we used a single polarized horn with a model of "PASTERNACK PE9851/2F-10" operating from 22 GHz to 33 GHz [20]. Since RA aperture size is comparable to feed horn size, to avoid significant feed blockage, the offset feeding method with the angle of θ = -35˚from normal direction is adopted. Moreover, the distance of the horn aperture to the RA surface is 27.5 mm. As an example, Fig. 9(a) and (b) illustrate the radiation patterns of the RA when the main beam is steered to the directions of φ = 90˚, θ = 45˚ and φ = 0˚, θ = 30˚, respectively. The realized gain is high in different beam directions.

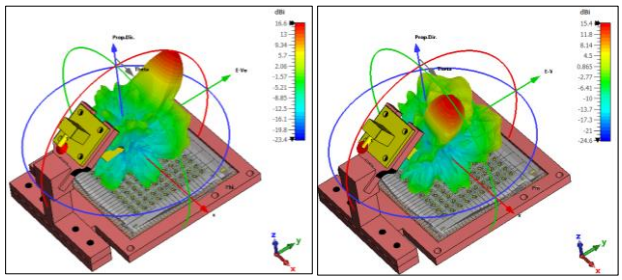

(a) (b)

Fig. 9. Simulated 3D radiation pattern of reflectarray with 30 µm LC thickness at 28 GHz for a) φ = 90, θ = 45˚and b) φ = 0, θ = 30˚

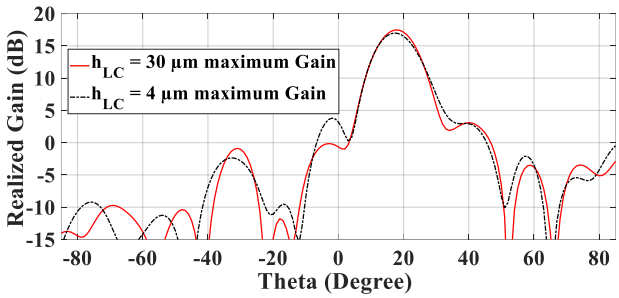

Fig. 10. Simulated radiation pattern of the RA for 30 µm and 4 um LC thickness at 28 GHz

The same simulation setup with only 4 µm LC thickness is also simulated to investigate the performance when we decrease the LC thickness. Fig. 10 shows the maximum simulated realized gain of the RA for both 30 µm and 4 µm LC thickness. As the offset feed is applied, the maximum gain appears around 18˚ with respect to boresight direction. The maximum realized gain is 17.5 dBi and 17 dBi at 28 GHz with 30 µm and 4 µm thick LC, respectively. The aperture efficiencies (AE) are 25.3% and 22.5%, respectively. Besides, since the thickness of the LC layer is small compared to wavelength, it is worth noting that a local mesh setting with at least 10 mesh cells across all axes is implemented in simulation setup to ensure an accurate result. Moreover, it is noticed that introducing the bias lines on the RA aperture reduces the realized gain by around 0.5 dB in the simulated results.

The limited range of phase shift of the unit cell, which is around 270º, is estimated to reduce the gain by 0.2 dB and increase the Side Lobe Level (SLL) by 2 dB, compared to the full range continuous phase shift of 360º from our studies.

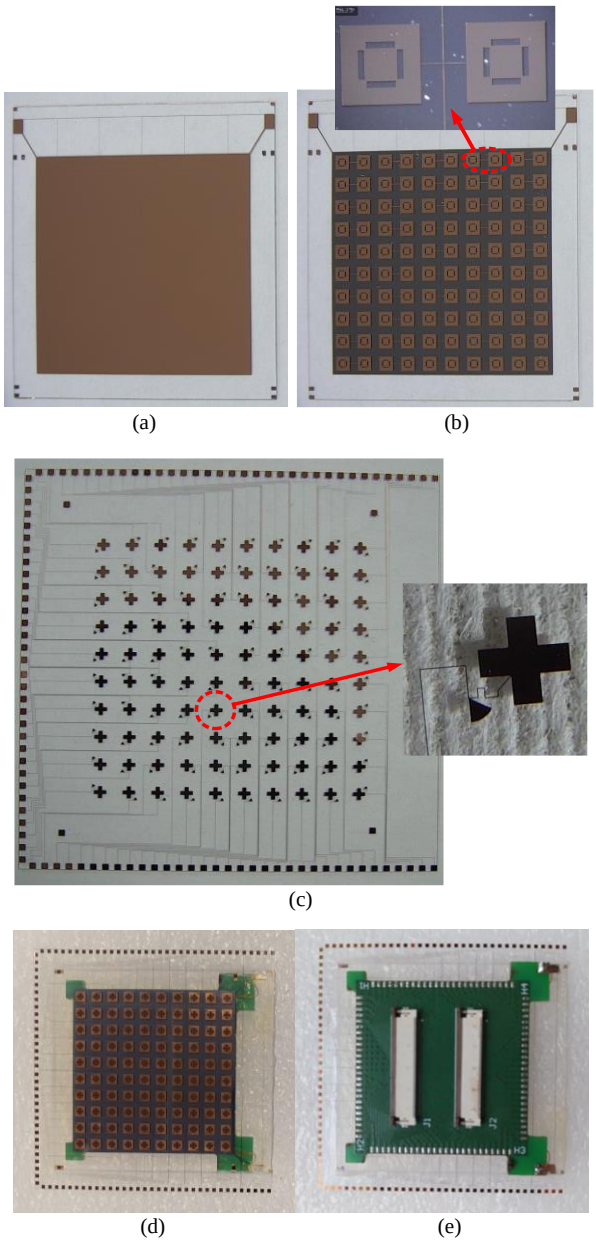

Fig. 11. 10×10 reflectarray with LC thickness of 30 µm: a) ground plane, b) square patch layer, c) cross patch layer and individual bias lines, d) top view of the assembled RA and e) back view of the assembled array with the attached PCB.

IV. Reflectarray Fabrication with 30 µm Thick LC

Due to the laboratory facility limitations, we have fabricated and manually assembled the RA with 30 µm thick LC instead of the 4 µm one. Fig. 11(a)-(c) shows the multiple metal layers of the fabricated samples. For the bottom glass substrate, the bottom metal layer is covered with a ground plane (Fig. 11(a)), while square patches connected to each other with narrow lines are printed on the top metal layer (Fig. 11(b)). To connect the square patch and ground plane layers, two big rectangular soldering pads (at the two up corners in Fig. 11 (a) and (b)) are added on each surface of the bottom glass. Before assembling the prototype, the soldering pads on two glass

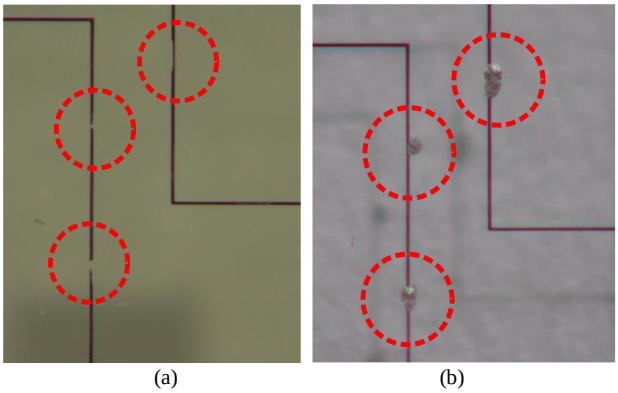

Fig. 12. a) Defects of small copper features after lift-off process, and b) cured copper features with conductive silver epoxy.

surfaces are connected via a 10-µm thick aluminum foil strip. In Fig. 11 (c) (or Fig. 1(c)), the bottom surface of the top glass substrate is patterned with cross patches connected to individual bias lines. The bias lines are distributed in the circumference of the top glass and then connected to some small soldering pads with symmetry in y-z plane. One edge of the top glass substrate is free of soldering pads, and it is aligned with the other glass substrate to facilitate assembly. In addition, small square copper marks are also added to further improve the localization accuracy of two glass substrates. Fig. 11(d) and (e) shows the assembled prototype. At the back of the RA, a PCB is attached on which two 50-pin FPC (Flat Flexible Cable) connectors are soldered. The solder pads on glass are then soldered to the PCB by wires.

A. *Fabrication process*

LC antenna fabrication requires several steps, which are elaborated here. The first step is creating the metal pattern made by photolithography, metallization, and lift-off process. As a rule of thumb, the metal layer thickness should be 3-5 times of skin depth δ (1.15-1.9 µm at 28 GHz) to minimize RF loss. However, due to fabrication facility limitations, here we used 600 nm copper thickness (which is 1.5×δ) to make a compromise between the lift-off process success and skin-depth loss. To ensure an accurate simulation, we can model the skin depth effect with surface impedance of the corresponding copper thickness in CST. The skin depth loss leads to only 0.5 dB gain reduction in the RA simulation. In general, the fabrication process yielded good precision and quality of the copper patterns. However, the non-ideal lift-off process caused the smallest features (bias lines) to fell off the substrate on some parts of the pattern. An example of this defect is illustrated in Fig. 12(a). A conductive silver epoxy has been applied on the defects to create the electrical connection. The epoxy is cured for 5 minutes in the oven with 150˚Celsius. Fig 12(b) shows the silver epoxy treatment spots, and the connections are tested afterward to validate the solution. However, these defects can be avoided with a better facility equipment.

After the lithography process and silver epoxy treatment, the copper-coated glasses are spin coated with approximately

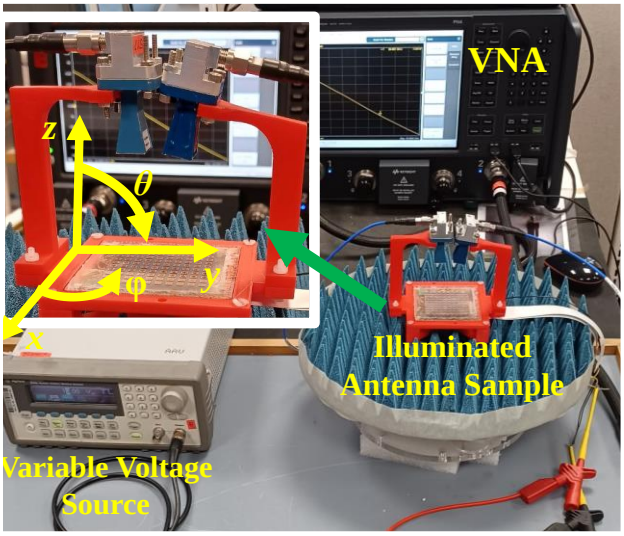

Fig. 13. Measurement setup for S12 measurement to obtain Phase-Voltage curve.

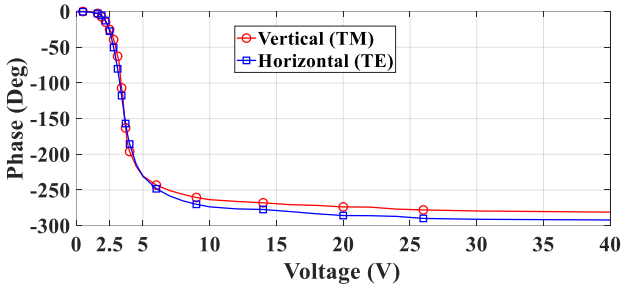

Fig. 14. Phase curve of S_{21} for vertical and horizontal polarization.

100 nm polyimide layer, and the surfaces are rubbed with a soft brush in y direction (following the coordinate axis of Fig. 8) to form the microgrooves that generates the anchoring force for initial alignment of LC directors. Next, the two substrates are assembled on top of each other with Ultraviolet (UV) glue that contains 30 μm polystyrene microspheres. The polystyrene microspheres ensure a smooth cavity thickness over the entire LC volume. The LC is then injected with vacuum filling technique and the sample is sealed to prevent LC leakage.

B. Reflection phase testing

A major step in the LC RA design is to obtain the relations between reflection phase and applied bias voltage. To obtain this relation, a free space measurement [7] should be carried out with one horn for illuminating and the other one for receiving. Several fixtures are manufactured with a 3D printer that holds two horns above the RA surface with different heights and incident angles. Two linear-polarized horn antennas with the same model as the above-mentioned are chosen: one for illuminating the unit cells and the other one for receiving the reflected wave. The measurement setup is illustrated in Fig. 13. First, the horns are assembled in a way that its electric field lies in the plane of the incident (TM wave) which we call the vertical polarization. The two horns

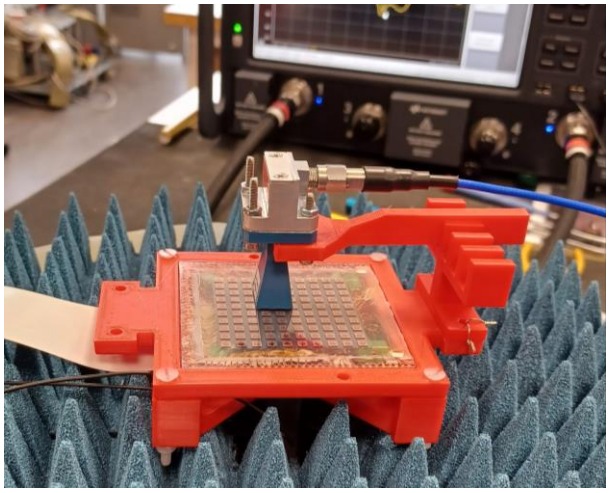

(a)

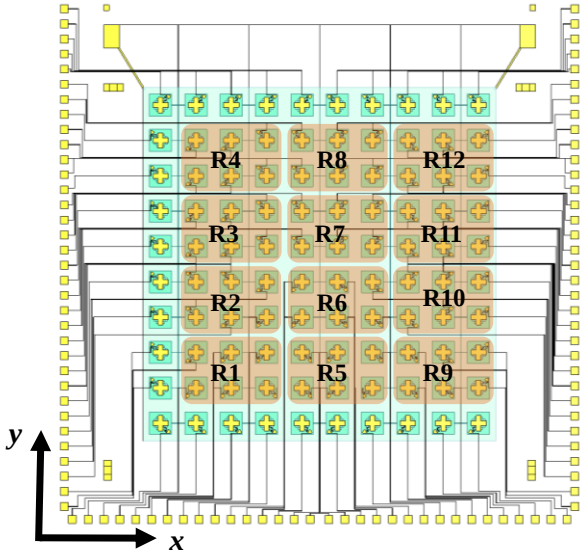

(b)

Fig. 15. a) Measurement setup for S_{11} measurement and b) the RA surface divided to 12 regions.

are connected to a Vector Network Analyzer (VNA) and all the unit cells are connected to a variable 1 kHz square voltage. By rotating the horn 90˚ around the propagation direction, the same procedure has been carried out with horizontal polarization (TE wave).

The measurement is repeated for different incident angles and horn heights including the same horn position used for the final RA setup (follow the coordinate axis of Fig. 13, $z = 27.5$ mm, $\varphi = 90^\circ$, and $\theta = -35^\circ$). However, only the result with the final RA setup is shown in Fig. 14. The phase of S_{21} at 28 GHz is provided as the applied voltage increases from 0 to 40 V for both polarizations. 281˚ and 290˚ phase shift can be observed for both vertical and horizontal polarizations, respectively. The measured results match with the simulation results of the oblique incident, obtained in Fig. 4 and 5. Although the discrepancy between measured and simulated phase shift is negligible, yet it was observed that decreasing the height of the horns would vary the phase range of the RA surface. One possible reason is that if the illumination horn

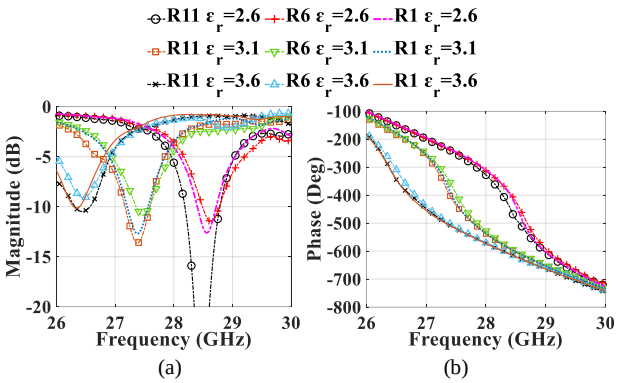

Fig. 16. Simulated S_{11} a) magnitude and b) phase for single horn measurement.

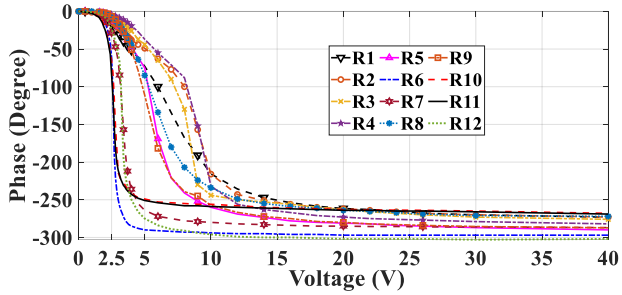

Fig. 17. Measured S_{11} phase of twelve regions at 28.5 GHz.

height is reduced, the received signal is from the contribution of one part of the RA surface instead of the whole. Moreover, by moving the RA surface in the x-y plane with the horn close to the surface, we can also observe a change in the resonant frequency at a fixed voltage. Therefore, the unit cells are not identical or not uniform across the whole RA surface.

After the investigation, the non-uniform response of the RA surface may be due to the imperfect manual assembling fabrication, which leads to a small difference in the LC thickness across the RA surface. Moreover, because the unbiased resonant frequency observed in the measurement is in the range of 29 GHz to 32 GHz for different regions, we can assume that the LC thickness is slightly higher than 30 µm. Another possible reason for the non-uniform unit cells could be the misalignment of top and bottom glass which can significantly change the resonant frequency. However, all the above fabrication errors can be avoided in massive production, where both assembling, and alignment tasks are done by machines precisely.

C. Obtaining the Correct Phase Curve

The fabricated RA surface is not uniform in this paper, and a similar issue may also occur in other research if manually assembling LC-based RA is required in labs. A novel method is proposed to locally investigate the phase behavior of the unit cells.

Given that the aperture of the horn we utilized is equal to the size of six unit cells, we can divide the entire RA surface into 12 regions and then perform a reflection/S_{11} measurement with the horn aperture. The measurement setup is shown in Fig.15(a) and the assigned regions are demonstrated in Fig.

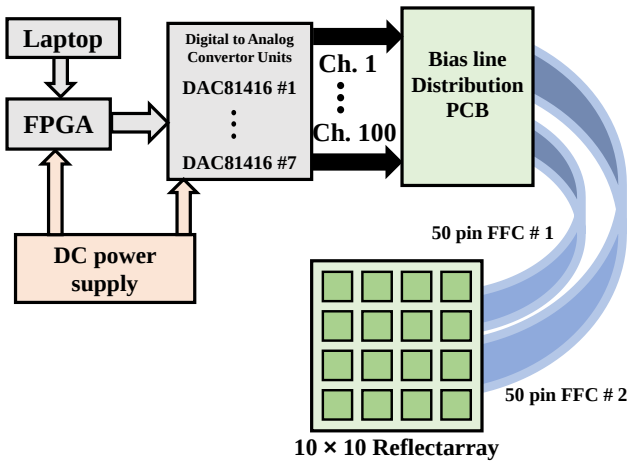

Fig. 18. Block diagram of voltage addressing scheme.

15(b). A 3D-printed fixture is designed for this purpose. To reduce any unknown parasitic effect from outside the RA active region, we avoided the edge elements as much as possible. Since we are stimulating the unit cells with a horn that has a flaring angle aperture with metallic walls, the boundary condition is different from the periodic boundary. Therefore, we simulated the measurement setup in CST Microwave Studio. As an example, Fig. 16 shows the S_{11} phase and magnitude for regions R1, R6, and R11 as we change the permittivity of the unit cells. It can be observed from Fig. 16(a) that the resonant frequency is shifted approximately 0.7 GHz compared to periodic boundary simulation which was displayed in Fig. 2. However, the relative phase curves do not change significantly for different regions and the maximum phase discrepancy at the center frequency is 40˚. Therefore, we can claim that moving the horn across the RA surface should not significantly change the relative phase and frequency between elements with the same permittivity.

At the next step, the S_{11} measurement for all regions are done by increasing the voltage of the whole array from 0 to 40 V and recording the reflection coefficient of the horn with a VNA. Fig. 17 demonstrates the reflective phase curves of the single horn measurement for 12 regions. The 0.7 GHz frequency shift that was observed in simulation is accounted for these curves. During the measurement, it was observed that not all the elements resonate around 28 GHz. In fact, the best overlap among regions is found to be around 28.5 GHz. However, for some of the regions, the maximum phase shift occurs above 28.5 GHz and thus they do not have any overlap. An interesting observation is the comparison of the curves in Fig. 14 and the curves of R6 and R7 in Fig. 17. It shows that the results obtained from S_{21} measurement in Fig. 14 are similar to the contribution of the central RA area.

D. Bias Control Circuit

Fig. 18 shows the block diagram of the control circuit that provides 100 individual variable AC bias voltages for the RA. Field Programmable Gate Array (FPGA) is used to control the

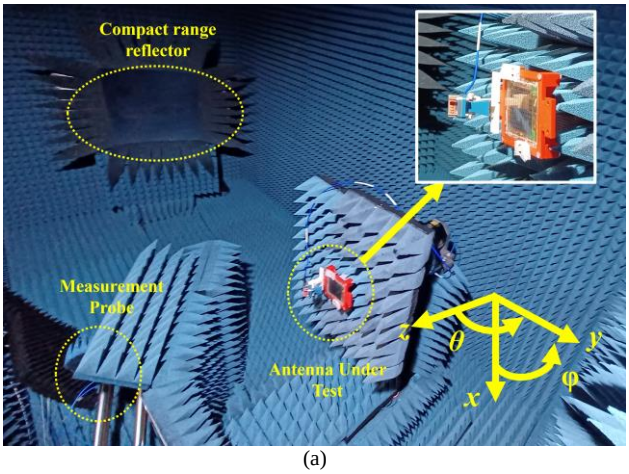

(a)

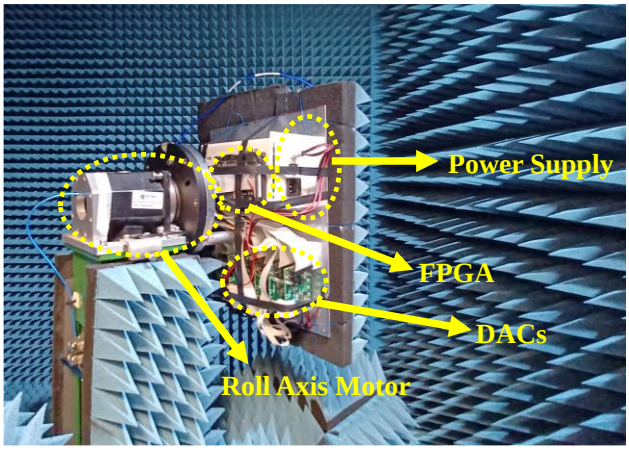

(b)

Fig. 19. Antenna Measurement Setup in anechoic chamber. a) front view of the mounted antenna, b) back of the mounted antenna

entire elements. It generates defined sequences according to the different beam directions and their corresponding phase distributions. Seven Digital-to-Analog Converters (DACs) of the model DAC81416 from Texas Instrument, each with 16 output channels, transform the digital sequences into 100 analog AC voltages. The DACs provide 1 kHz zero to 40 V with 16-bit resolution.

Since the phase curves of some regions in Fig. 18 are extremely steep, we need to make sure that the DAC can handle this sharp voltage change properly. The first point is that the DAC has 16-bit resolution which corresponds to 0.61 mV for 0 V to 40 V range. The phase shift shows a steep curve in 2-4 V. Therefore, the DACs can provide voltages values with approximately 3270 steps in this span. Another important point is the error between desired voltage value and the actual voltage value which can be describe by Total Unadjusted Error (TUE) of the DAC. For the model of "DAC81416", TUE is ±0.01% of the Full Scale Range (FSR). Therefore, the error for 40 V range is ±0.004 V. The sharpest change in all the phase curves is for R6 in Fig. 17 for 2.5 V to 3 V. In this span, we have 185º phase variation. If we divide the voltage range by the TUE (0.5/0.004 = 125) and then divide the maximum phase range by that value (185º / 125 = ±1.48º), the phase error would be ±1.48º which does not have any considerable effect on radiation performance.

V. Radiation Pattern Measurements

A. Measurement Setup

To generate a high directivity beam, the phase distribution on the surface of RA should be provided in a way that transforms the incoming spherical wave of feed horn source into a plane wave in any given direction. Conventionally, a single curve can be used to calculate the phase distribution for all the elements of the RA for a given beam direction. However, since the resonant frequency and phase curve of the elements are different here, we can divide the one hundred elements into use 12 regions and use the curve of Fig. 17 in each region. It should be noted that the phase of edge elements which is not covered in Fig. 15(b) is calculated based on the curves of their adjacent regions. Fig. 19 shows the complete measurement setup in an anechoic chamber. Due to the lack of a dual-polarized horn in the 28 GHz band, dual polarization measurement should be done for each polarization separately. In the first step, the single polarized feed horn mentioned in Section III is assembled in a way that its electric field lies in the plane of incident ($\varphi = 90^\circ$) which we call the vertical polarization (TM wave). For the orthogonal polarization test, the feed can be rotated 90° around the propagation axis. Following the coordinate system of Fig. 19 (a) and assuming the origin is at the center of the RA surface, the feed position is at (x, y, z) = (0 mm, -18.5 mm, 27 mm) with $\varphi = 90^\circ$ and $\theta = -35^\circ$.

B. Radiation Measurement Results

As mentioned above, the maximum phase difference for most of the region has an overlap around 28.5 GHz. Fig. 20 (a) and (b) illustrates the measured beam-steering radiation patterns of vertical polarization for $\varphi = 90^\circ$ plane and $\varphi = 0^\circ$ plane at 28.5 GHz. The maximum realized gain for vertical polarization occurs around $\theta = 15^\circ$ off-boresight which is 14.2 dBi. The maximum simulated realized gain is 17.5 dBi which shows 3.3 dB gain reduction in the measurement. The gain discrepancy and high SLL are mainly due to the significant phase errors along with large reflective amplitude variation introduced by the nonuniform unit cell distribution. The non-uniformity leads to different resonant frequencies across the RA surface. However, using a separate curve for each region can compensate for this error, but it cannot be eliminated entirely. Another reason for the gain discrepancy is the skin depth loss which could be eliminated by increasing the copper thickness in lithography process. The main beam in $\varphi = 90^\circ$ plane is steered from -10° to +45° with 3-dB gain roll-off, while in $\varphi = 0^\circ$ plane the beam can be steered from +45° to -45°. Simulated radiation pattern is also shown in Fig. 20 (c) and (d), which shows a scanning range of -15 to +50 in $\varphi = 0^\circ$ plane, and ±50º in $\varphi = 0^\circ$ plane.

The measured beam-steering radiation patterns for horizontal polarization is illustrated in Fig. 21 (a) and (b). The main beam in $\varphi = 90^\circ$ plane is steered from -10° to +50° with 3-dB gain roll-off, while in $\varphi = 0^\circ$ plane the beam can be steered

TABLE I
COMPARISON OF THE PROPOSED REFLECTARRAY AND PRIOR STUDIES

Ref	Frequency (GHz)	Polarization	Aperture efficiency (%)	3-dB Gain Bandwidth	Scanning range and direction (°)	LC thickness (λ)
[12]	24	Single	23	16.5%	±45°, 2D	0.04λ
[18]	21	Single	5.8	NA	0 to 60°, 1D	5.6×10^{-4}λ
[8]	100	Single	1.8	8%	0 to 55°, 1D	0.026 λ
[11]	78	Single	—	5%	±6°, 1D	0.013 λ
[6]	35	Single	9.2	NA	±20°, 1D	0.014 λ
This work 30 μm thick, Mes. 30 μm thick, Sim.	 28.5 28	 Dual Dual	 12.5 25.3	 4.5% 7% (Ver, Hor) 5.7%, 6.5% (Ver, Hor)	 ±45°, 2D ±50°, 2D	 0.0028 λ 0.0028 λ
This work 4 μm thick, Sim.	 28	 Dual	 22.5	 6.2%, 6.4% (Ver, Hor)	 ±50°, 2D	 3.73×10^{-4}λ

NA: Not available

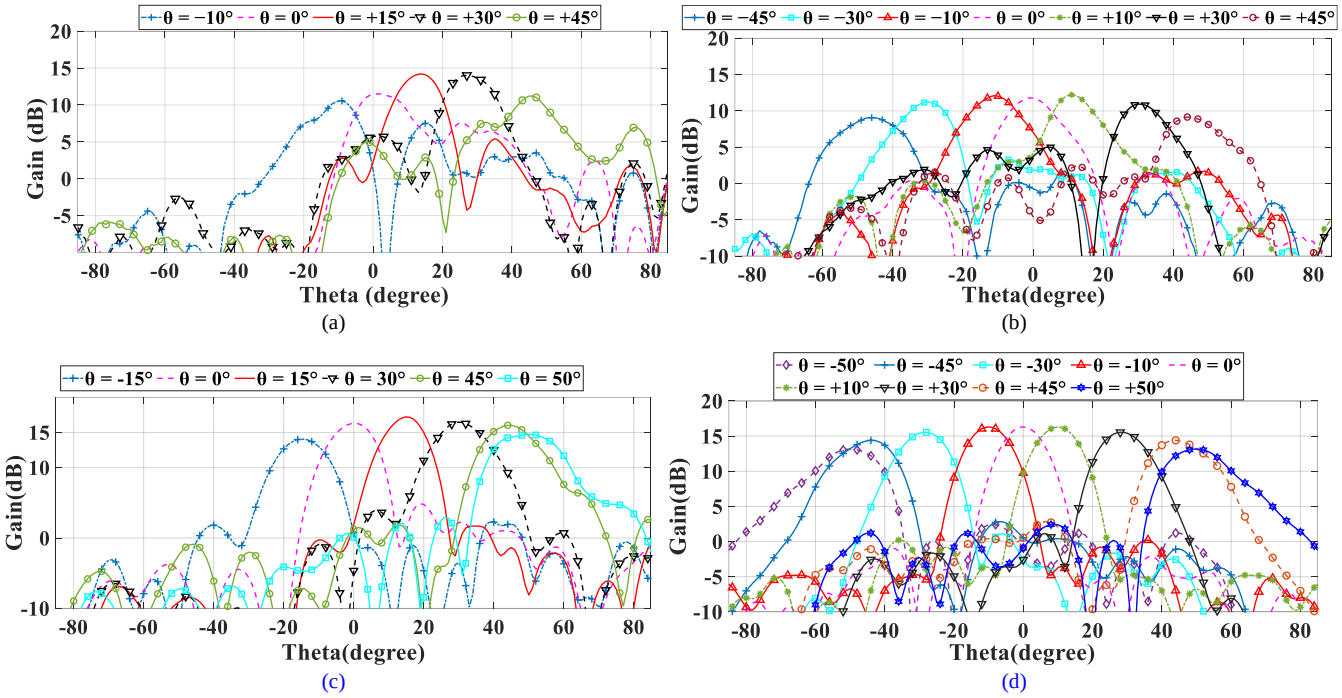

Fig. 20. Measured radiation pattern of vertical polarization for a) φ = 90˚ and b) φ = 0˚ and simulated radiation pattern of vertical polarization for c) φ = 90˚ and d) φ = 0˚

from +45˚ to -45˚. Simulated radiation pattern is also shown in Fig. 21 (c) and (d), which shows a scanning range of -15 to +50 in φ = 0˚ plane, and ±50° in φ = 0˚ plane. The maximum gain in horizontal polarization reaches 14.6 dBi in θ = 15˚ which corresponds to 12.5% aperture efficiency. Since the radiation pattern of the feed horn is not identical in E and H-plane, and each phase curve is an approximation for a group of unit cells, a slight change in phase and amplitude distribution can lead to the difference in far-field radiation patterns for vertical and horizontal polarization. Also, the difference in TE and TM polarization responses shown in Fig. 4 and 5 introduce phase errors for vertical and horizontal polarization. Due to the symmetry of the unit cell, if a non-offset feed method is adopted, the non-equal TE and TM response effects can be significantly reduced. Moreover, the anisotropic nature of LC discussed in Section II could also cause a phase error and the concomitant change of radiation pattern in dual polarization could appear. It is worth mentioning that the discrimination between Co and Cross polarization of the fabricated antenna is over 10 dB for all the frequencies and beam directions, and over 15 dB in most of the cases. The maximum realized gain over frequency for both polarizations is demonstrated in Fig. 22. A measured 3-dB gain bandwidth of 7% and 4.5% for horizontal and vertical polarization is observed, respectively.

As explained in Section IV.B, the LC thickness is the key factor of response time. In this prototype with around 30 μm thick LC, the time of steering between two beams from +45˚ to -45˚ is approximately 3 s.

A comparison with previous studies is presented in Table I. Compared to the study presented in [12], the proposed study here achieved dual polarization and a much smaller LC thickness with a comparable aperture efficiency. Compare to [18], which has a thinner LC layer, the presented study here

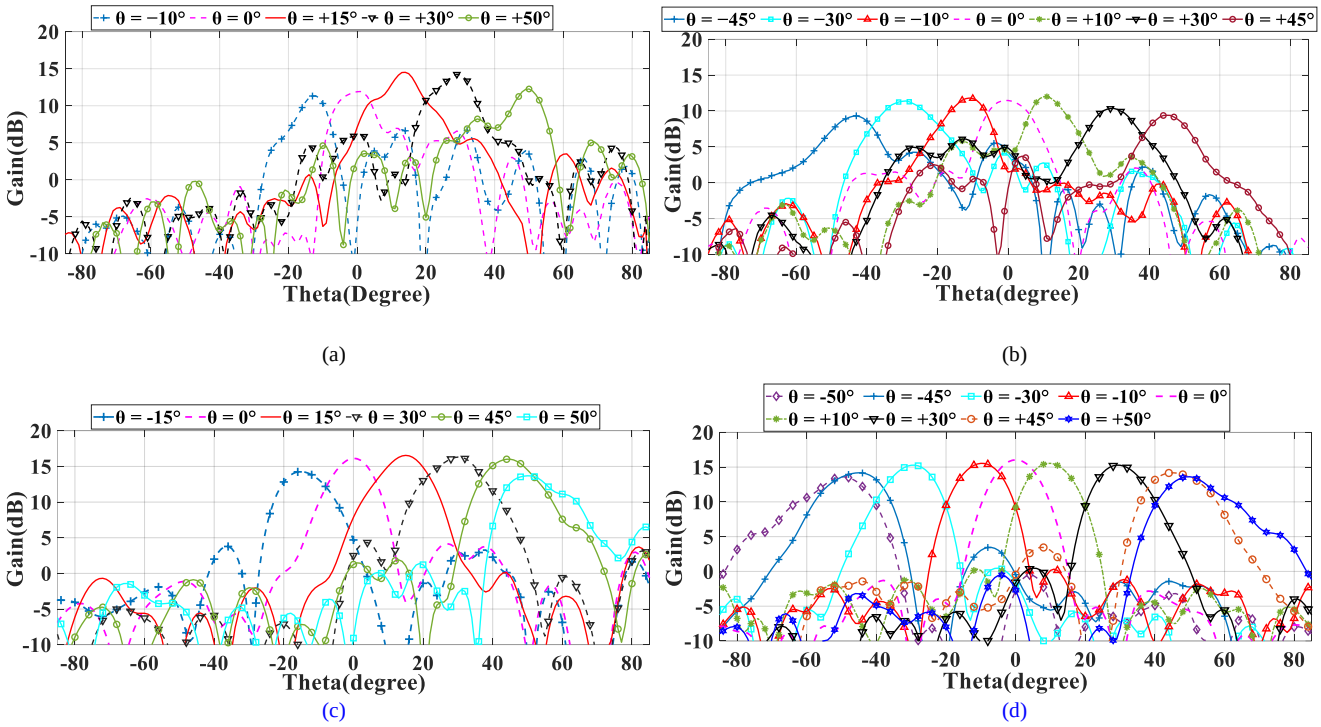

Fig. 21. Measured radiation pattern of horizontal polarization for a) φ = 90˚ and b) φ = 0˚ and simulated radiation pattern of horizontal polarization for c) φ = 90˚ and d) φ = 0˚

achieved a higher aperture efficiency and 2D beam-steering with dual polarization. The measured results of the fabricated prototype prove the validity of the dual-polarized 2D beam-steering based on 30 µm LC thickness. Presented simulation data in Fig. 8 reveals that the proposed technique can also achieve the good electrical performance with 4 µm LC thickness (that is not possible to be assembled and fabricated manually). In general, response time decreases with thickness reduction of the same LC material. Therefore, the LC thickness has been compared. Among all the other studies, the presented study is superior in case of polarization, efficiency, scanning range and LC thickness.

Although we have discrepancies between measurement and simulation, by using a mature LCD fabrication technology, the errors can be rectified, and we can reach a good performance index in case of fabrication cost, aperture efficiency, scan range etc., that is comparable to recent PIN or Varactor diode-based beam-steering techniques like those presented in [1][21]-[23]. Moreover, if a low loss LC mixture [13] is used, the presented study can reach even over 30% aperture efficiency. It must be mentioned that two of the promising features of LC are the unlimited operating frequency range and low-cost mass-production which makes the LC technology an appealing solution for future reconfigurable surface applications.

VI. Conclusion

In this paper, a LC unit cell configuration has been proposed which proves the potential of reducing the LC thickness significantly to improve the response time issue in LC-based RAs. The working mechanism and dual-polarization scheme

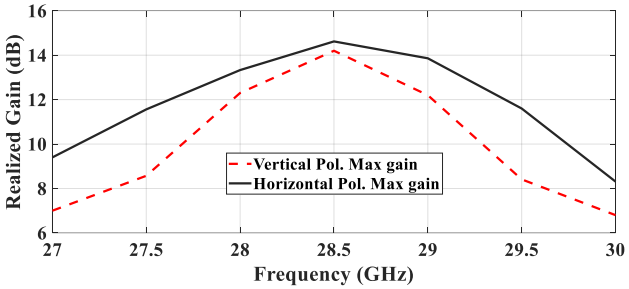

Fig. 22. Maximum realized gain over frequency for vertical and horizontal polarization.

of the design have been discussed. The unit cells with 30 µm and 4 µm thick LC have been simulated and their corresponding RA performance has been presented. A 10 × 10 reflectarray with 30 µm LC thickness has been fabricated with 2D bias addressing. The fabrication issues have been discussed, and a novel method has been proposed to measure the reflection phase of the RA. Based on the reflection phase measurements, far-field pattern measurements have been carried out. The 2D beam scanning has been achieved for both polarizations successfully and the proposed work has been compared with recent studies.

References

[1] X. Pan, F. Yang, S. Xu and M. Li, "A 10240-Element Reconfigurable Reflectarray With Fast Steerable Monopulse Patterns," *IEEE Trans. Antennas Propag.*, vol. 69, no. 1, pp. 173-181, Jan. 2021.

[2] M. E. Trampler, R. E. Lovato, and X. Gong, "Dual-Resonance Continuously Beam-Scanning X-Band Reflectarray Antenna," *IEEE Trans. Antennas Propag.*, vol. 68, no. 8, pp. 6080-6087, Aug. 2020.

[3] K. K. Karnati, M. E. Trampler and X. Gong, "A Monolithically BST-

Integrated Ka-Band Beamsteerable Reflectarray Antenna," *IEEE Trans. Antennas Propag.*, vol. 65, no. 1, pp. 159-166, Jan. 2017.

[4] Y. Zhao et al., "A Digital Metamaterial of Arbitrary Base Based on Voltage Tunable Liquid Crystal," *IEEE Access*, vol. 7, pp. 79671-79676, 2019.

[5] W. Hu et al., "Design and Measurement of Reconfigurable Millimeter Wave Reflectarray Cells With Nematic Liquid Crystal," *IEEE Trans. Antennas Propag.*, vol. 56, no. 10, pp. 3112-3117, Oct. 2008.

[6] J. F. and R. J. A. Moessinger, R. Marin, S. Mueller, "Electronically reconfigurable reflectarrays with nematic liquid crystals," *Electron. Lett.*, vol. 42, no. 16, pp. 40–41, 2006.

[7] S. -Y. Sun et al., "Electronically Tunable Liquid-Crystal-Based F-Band Phase Shifter," *IEEE Access*, vol. 8, pp. 151065-151071, 2020.

[8] G. Perez-Palomino et al., "Design and Demonstration of an Electronically Scanned Reflectarray Antenna at 100 GHz Using Multiresonant Cells Based on Liquid Crystals," I*EEE Trans. Antennas Propag.*, vol. 63, no. 8, pp. 3722-3727, Aug. 2015.

[9] G. Perez-Palomino et al., "Design and Experimental Validation of Liquid Crystal-Based Reconfigurable Reflectarray Elements With Improved Bandwidth in F-Band," *IEEE Trans. Antennas Propag.*, vol. 61, no. 4, pp. 1704-1713, April 2013.

[10] S. Gao et al., "Tunable Liquid Crystal Based Phase Shifter with a Slot Unit Cell for Reconfigurable Reflectarrays in F-Band," *Applied Sciences*, vol. 8, no. 12, p. 2528, Dec. 2018

[11] S. Bildik, S. Dieter, C. Fritzsch, W. Menzel and R. Jakoby, "Reconfigurable Folded Reflectarray Antenna Based Upon Liquid Crystal Technology," *IEEE Trans. Antennas Propag.*, vol. 63, no. 1, pp. 122-132, Jan. 2015.

[12] X. Li et al., "Broadband Electronically Scanned Reflectarray Antenna With Liquid Crystals, " *IEEE Antenn. Wireless Propag. Lett.*, vol. 20, no. 3, pp. 396-400, March 2021.

[13] R. Jakoby, A. Gaebler, and C. Weickhmann, "Microwave Liquid Crystal Enabling Technology for Electronically Steerable Antennas in SATCOM and 5G Millimeter-Wave Systems," *Crystals*, vol. 10, no. 6, p. 514, Jun. 2020.

[14] K. K. Karnati, Y. Yusuf, S. Ebadi and X. Gong, "Theoretical Analysis on Reflection Properties of Reflectarray Unit Cells Using Quality Factors," *IEEE Trans. Antennas Propag.*, vol. 61, no. 1, pp. 201-210, Jan. 2013.

[15] Z. Yin et al., "Fast-Tunable Terahertz Metamaterial Absorber Based on Polymer Network Liquid Crystal," *Applied Sciences*, vol. 8, no. 12, p. 2454, Dec. 2018.

[16] J. Yang et al., "Fully Electronically Phase Modulation of Millimeter-Wave via Comb Electrodes and Liquid Crystal," *IEEE Antenn. Wireless Propag. Lett.*, vol. 20, no. 3, pp. 342-345, March 2021.

[17] H. Kim, J. Kim and J. Oh, "Liquid-Crystal-Based X-Band Reactively Loaded Reflectarray Unit Cell to Reduce Reflection Loss," *IEEE Antenn. Wireless Propag. Lett.*, vol. 20, no. 10, pp. 1898-1902, Oct. 2021.

[18] W. Zhang, Y. Li and Z. Zhang, "A Reconfigurable Reflectarray Antenna With an 8 μm-Thick Layer of Liquid Crystal," *IEEE Trans. Antennas Propag.*, vol. 70, no. 4, pp. 2770-2778, April 2022.

[19] H. Lu, S. Jing, T. Xia, J. Yang, Z. Yin, G. Deng, "Measurement of LC dielectric constant at lower terahertz region based on metamaterial absorber," *IEICE Electronics Express*, 2017, vol. 14, no. 12, pp. 20170469, June. 2017.

[20] "https://www.pasternack.com/standard-gain-horn-waveguide-size-wr34-10-db-gain-292mm-female-pe98512f-10-p.aspx" .

[21] B. J. Xiang, X. Dai and K. -M. Luk, "A Wideband Low-Cost Reconfigurable Reflectarray Antenna With 1-Bit Resolution," *IEEE Transactions on Antennas and Propagation*, vol. 70, no. 9, pp. 7439-7447, Sept. 2022.

[22] H. Luyen, Z. Zhang, J. H. Booske and N. Behdad, "Wideband, Beam-Steerable Reflectarray Antennas Exploiting Electronically Reconfigurable Polarization-Rotating Phase Shifters," *IEEE Transactions on Antennas and Propagation*, vol. 70, no. 6, pp. 4414-4425, June 2022.

[23] B. Xi, Y. Xiao, K. Zhu, Y. Liu, H. Sun and Z. Chen, "1-Bit Wideband Reconfigurable Reflectarray Design in Ku-Band" *IEEE Access*, vol. 10, pp. 4340-4348, 2022.